A comparison of nonlocal continuum and discrete dislocation plasticity predictions

Bittencourt, E.; Needleman, A.; Gurtin, M.E.; Giessen, E. van der

Published in:
Journal of the Mechanics and Physics of Solids

DOI:
10.1016/S0022-5096(02)00081-9

Publication date:
2003


PERGAMON

Journal of the Mechanics and Physics of Solids
51 (2003) 281–310

JOURNAL OF THE
MECHANICS AND
PHYSICS OF SOLIDS

www.elsevier.com/locate/jmps

A comparison of nonlocal continuum and discrete dislocation plasticity predictions

E. Bittencourt[a], A. Needleman[a,*], M.E. Gurtin[b], E. Van der Giessen[c]

[a] *Division of Engineering, Brown University, Providence, RI 02912, USA*
[b] *Department of Mathematics, Carnegie Mellon University, Pittsburgh, PA 15213, USA*
[c] *Department of Applied Physics, University of Groningen, Nyenborgh 4, 9747 AG Groningen, The Netherlands*

Received 29 January 2002; received in revised form 19 July 2002; accepted 30 July 2002

Abstract

Discrete dislocation simulations of two boundary value problems are used as numerical experiments to explore the extent to which the nonlocal crystal plasticity theory of Gurtin (J. Mech. Phys. Solids 50 (2002) 5) can reproduce their predictions. In one problem simple shear of a constrained strip is analyzed, while the other problem concerns a two-dimensional model composite with elastic reinforcements in a crystalline matrix subject to macroscopic shear. In the constrained layer problem, boundary layers develop that give rise to size effects. In the composite problem, the discrete dislocation solutions exhibit composite hardening that depends on the reinforcement morphology, a size dependence of the overall stress–strain response for some morphologies, and a strong Bauschinger effect on unloading. In neither problem are the qualitative features of the discrete dislocation results represented by conventional continuum crystal plasticity. The nonlocal plasticity calculations here reproduce the behavior seen in the discrete dislocation simulations in remarkable detail.

Keywords: Constitutive behavior; Crystal plasticity; Dislocations; Metallic materials

1. Introduction

Classical plasticity theories predict a size independent response, while a considerable body of experimental evidence, e.g. Ebeling and Ashby (1966), Brown and Ham

* Corresponding author. Tel.: +1-401-863-2863; fax: +1-401-863-1157.
E-mail address: needle@engin.brown.edu (A. Needleman).

0022-5096/03/$ - see front matter
PII: S0022-5096(02)00081-9

(1971), De Guzman et al. (1993), Fleck et al. (1994), Ma and Clarke (1995) and Stölken and Evans (1998), has accumulated that inhomogeneous plastic flow in crystalline solids is inherently size dependent over a scale that ranges from a fraction of a micron to a hundred microns or so—with smaller generally being harder. There is an intimate connection between size effects and gradients of plastic deformation, as was recognized by Nye (1953). This connection is through the concept of geometrically necessary dislocations (Nye, 1953; Ashby, 1970), which is, in essence, a measure of density of net Burgers vector.

Predicting a size effect has provided the motivation for much work on developing phenomenological nonlocal theories of plastic flow. There are a variety of dislocation mechanisms that give rise to scale effects, see e.g. Mughrabi (1983), Aifantis (1984), Ortiz et al. (2000), Busso et al. (2000). The focus here is on phenomenological models that incorporate a length scale aimed at modeling the nonlocal effects arising from geometrically necessary dislocations, as, for example, in Fleck and Hutchinson (1993, 1997, 2001), Acharya and Bassani (2000), Shu and Fleck (1999), Gao et al. (1999), Huang et al. (2000), Gurtin (2000, 2002) and Svendsen (2002). Length scale effects are incorporated in various ways, in the flow strength, in the hardening or in the free energy, and this has a profound effect on the boundary value problem structure that emerges. Although the applicability of these approaches is ultimately decided by comparing their predictions with experiment, comparisons with the predictions of a direct dislocation based description of plastic flow can be more detailed and useful in assessing the validity of the various nonlocal formulations.

In this regard, it bears emphasis that although much of the focus on geometrically necessary dislocations has been related to size effects, another consequence of the presence of geometrically necessary dislocations is a possible long range stress field which affects hardening and the Bauschinger effect on unloading. In this paper, we compare the predictions of the nonlocal crystal plasticity theory proposed by Gurtin (2002) with the behavior obtained from a discrete dislocation description of plastic flow. Two boundary value problems for a single crystal are considered: simple shear of a constrained layer (Shu et al., 2001) and a model composite material subject to simple shear (Cleveringa et al., 1997, 1998, 1999a). The constrained layer problem is such that a local plasticity theory would predict uniform shear strain in the layer. Discrete dislocation plasticity gives rise to very different behavior in the constrained layer problem depending on whether the crystal is oriented for single slip or symmetric double slip. In single slip, the shear stiffness in the plastic range is of the order of the elastic shear modulus while in symmetric double slip the effective shear stiffness has a much smaller value, of the order of the flow strength. In both single and double slip, the shear strain in the layer is not uniform, but the boundary layers that develop in double slip are much more pronounced than those that develop in single slip and evolve with increasing deformation. The aggregate stress–strain response predicted by discrete dislocation plasticity depends sensitively on the reinforcement morphology. Furthermore, a size dependence and a large Bauschinger effect are seen for one reinforcement morphology but not for another.

We begin by outlining the nonlocal plasticity theory proposed in Gurtin (2002), restricted to infinitesmal deformations and rate independent material behavior. Two

sources of hardening are accounted for in this theory; dissipative hardening associated with an increase in slip resistance and energetic hardening associated with an increase in free energy due to a density of geometrically necessary dislocations. The discretization of the nonlocal theory within a finite element framework and the implicit time integration procedure are then described. Although the theoretical framework and numerical implementation are, in principle, fully three dimensional, both the constrained layer and the model composite material problems are plane strain problems. Both ideally plastic and hardening crystals are considered. An analytical solution is presented for a single crystal with two symmetrically oriented slip systems subject to simple shear. This solution provides a check on the numerical procedure and reveals the coupling between dissipative and energetic hardening needed to capture the features seen in the discrete dislocation results.

2. Nonlocal-plasticity: formulation and numerical implementation

2.1. Formulation

The calculations are based on the nonlocal theory of crystal plasticity due to Gurtin (2002) specialized to circumstances where geometry changes are negligible and the material response is rate independent. The governing equations are summarized using Cartesian tensor notation.

The gradient of the displacement vector, u_i, is written as the sum of elastic and plastic parts

$$u_{i,j} = u^{\mathrm{e}}_{ij} + u^{\mathrm{p}}_{ij}. \tag{1}$$

Attention is confined to crystalline solids for which plastic deformation takes place by crystallographic slip on a specified set of slip planes. With $s_i^{(\beta)}$ and $m_i^{(\beta)}$ unit vectors specifying the slip direction and the slip plane normal, respectively, for slip system β, the plastic part of the displacement gradient is given by

$$u^{\mathrm{p}}_{ij} = \sum_{\beta} \gamma^{(\beta)} s_i^{(\beta)} m_j^{(\beta)} \tag{2}$$

with $\gamma^{(\beta)}$ the total slip on the system β. (We consistently use Greek superscripts, without the summation convention, to label the slip systems.)

A motivation for the nonlocal formulation in Gurtin (2002) stems from the fact that plastic deformation in crystalline solids arises from the motion of dislocations, which are line defects characterized by a Burgers vector b_i. Each dislocation gives rise to a stress field that, within the context of linear elasticity, falls off as $1/r$ where r is the distance from the dislocation line. If the dislocations are randomly oriented with Burgers vectors $+b_i$ and $-b_i$ being equally likely, at distances far from these opposite signed dislocations, their stress fields cancel. Hence, if the net Burgers vector in a large (compared with the dislocation spacing) piece of dislocated crystal is zero, there are no long range stresses associated with the dislocation structure. There is then no increase in free energy associated with the average tractions and displacements on the surface

of this piece of the crystalline solid, although there is a free energy increase that scales with length of dislocation line. On the other hand, if the dislocation structure has a net Burgers vector, the tractions on the surface of the piece of dislocated crystal are not negligible due to the slow $1/r$ decrease and there is an increase in free energy associated with the average traction. This increase in free energy scales with the net Burgers vector.

The displacement gradient $u_{i,j}$ satisfies the compatibility relation

$$\oint_C u_{i,j}\,\mathrm{d}x_j = 0, \tag{3}$$

but neither u^{e}_{ij} nor u^{p}_{ij} do separately. This observation allows one to characterize the net Burgers vector B_i with respect to a closed loop C in the crystal through the integral

$$B_i = \oint_C u^{\mathrm{p}}_{ij}\,\mathrm{d}x_j = \oint_S \alpha_{ij} v_j\,\mathrm{d}S \tag{4}$$

in which S is any surface with boundary C and v_i is the unit normal field for S suitably oriented with respect to C. The tensor α_{ij}, which is often referred to as Nye's dislocation density tensor (Nye, 1953) or as the density of geometrically necessary dislocations, is given by the explicit relation

$$\alpha_{ij} = \sum_\beta e_{jkl}\gamma^{(\beta)}_{,k} s^{(\beta)}_i m^{(\beta)}_l, \tag{5}$$

where e_{ipq} is the alternating tensor. This relation can be rewritten to show that α_{ij} depends on $\gamma^{(\beta)}_{,k}$ at most through derivatives of $\gamma^{(\beta)}$ in the βth slip-plane (Fleck et al., 1994).

Because of the nonstandard nature of the theory, the derivation of the balance laws is based on a principle of virtual work in which fields $\pi^{(\beta)}$ and $\xi^{(\beta)}_i$ work-conjugate to slips and slip gradients are introduced:

$$\int_B \left[\sigma_{ij}\delta u^e_{ij} + \sum_\beta \pi^{(\beta)}\delta\gamma^{(\beta)} + \sum_\beta \xi^{(\beta)}_i \delta\gamma^{(\beta)}_{,i}\right] \mathrm{d}V$$

$$= \int_{\partial B_q} \sum_\beta q^{(\beta)}\delta\gamma^{(\beta)}\,\mathrm{d}A + \int_{\partial B_t} t_i \delta u_i\,\mathrm{d}A. \tag{6}$$

Here σ_{ij} is the standard stress tensor with $\sigma_{ij} = \sigma_{ji}$.

Using Eqs. (1) and (2), the left-hand side of (6) can be written as

$$\int_B \left[\sigma_{ij}\delta u_{i,j} + \sum_\beta (\pi^{(\beta)} - \tau^{(\beta)})\delta\gamma^{(\beta)} + \sum_\beta \xi^{(\beta)}_i \delta\gamma^{(\beta)}_{,i}\right] \mathrm{d}V,$$

where

$$\tau^{(\beta)} = m^{(\beta)}_i \sigma_{ij} s^{(\beta)}_j \tag{7}$$

represents the resolved shear. Since Eq. (6) must hold for variations δu and $\delta\gamma^{(\beta)}$, we are led to the classical balance

$$\sigma_{ij,j} = 0 \tag{8}$$

to a microforce balance

$$\pi^{(\beta)} - \tau^{(\beta)} - \xi^{(\beta)}_{i,i} = 0 \tag{9}$$

and to boundary conditions in which either

$$t_i = \sigma_{ij} n_j \quad \text{or} \quad u_i \tag{10}$$

and either

$$q^{(\beta)} = \xi^{(\beta)}_i n_i \quad \text{or} \quad \gamma^{(\beta)} \tag{11}$$

are prescribed at each point of the boundary. Subsequently, a boundary condition of the form $\gamma^{(\beta)} = 0$ is referred to as a micro-clamped boundary condition and a boundary condition of the form $q^{(\beta)} = 0$ is termed a micro-free boundary condition.

To account for the dependence of the free energy Ψ on the net Burgers vector, Ψ is assumed to have the form (Gurtin, 2002)

$$\Psi(\varepsilon^{\mathrm{e}}_{ij}, \alpha_{ij})$$

with

$$\varepsilon^{\mathrm{e}}_{ij} = \tfrac{1}{2}(u^{\mathrm{e}}_{ij} + u^{e}_{ji}). \tag{12}$$

Thermodynamical arguments then lead to the classical relation

$$\sigma_{ij} = \frac{\partial \Psi}{\partial \varepsilon^{\mathrm{e}}_{ij}} \tag{13}$$

in conjunction to the following relation for the "microstress" $\xi^{(\beta)}_i$ (Gurtin, 2002):

$$\xi^{(\beta)}_i = e_{ipq} m^{(\beta)}_p T_{qr} s^{(\beta)}_r \tag{14}$$

with

$$T_{ji} = \frac{\partial \Psi}{\partial \alpha_{ij}}. \tag{15}$$

T_{ji} represents a defect stress tensor; note that α_{ij} and T_{ji} are not generally symmetric.

Thermodynamics requires also that $\sum_\beta \pi^{(\beta)} \dot{\gamma}^{(\beta)} \geqslant 0$. Consistent with this inequality and with rate independence we assume that, constitutively,

$$\pi^{(\beta)} = \varphi^{(\beta)} \operatorname{sgn} \dot{\gamma}^{(\beta)} \tag{16}$$

with $\varphi^{(\beta)} > 0$, the slip resistance on β, governed by an equation of the form

$$\dot{\varphi}^{(\beta)} = \sum_\kappa h^{(\beta\kappa)}(\varphi^{(1)}, \varphi^{(2)}, \ldots, \varphi^{(N)}, \alpha_{ij}) |\dot{\gamma}^{(\kappa)}| \quad (h^{(\beta\kappa)} \geqslant 0). \tag{17}$$

Here $(\dot{\ })$ denotes differentiation with respect to some monotonically increasing time-like parameter that characterizes the loading history.

Constitutive equation (16) applies only when there is flow on β, so that $\dot{\gamma}^{(\beta)} \neq 0$. We stipulate that the response on β be elastic ($\dot{\gamma}^{(\beta)} = 0$) when

$$|\tau^{(\beta)} + \xi^{(\beta)}_{i,i}| < \varphi^{(\beta)}. \tag{18}$$

In this case $\pi^{(\beta)}$ is considered indeterminate, so that the microforce balance (9) is satisfied automatically.

The free energy $\Psi(\varepsilon^{\mathrm{e}}_{ij}, \alpha_{ij})$ is taken to have the additive quadratic form

$$\Psi = \tfrac{1}{2} L_{ijlk} \varepsilon^{\mathrm{e}}_{ij} \varepsilon^{\mathrm{e}}_{kl} + \tfrac{1}{2} \ell^2 \pi_0 \alpha_{ij} \alpha_{ij}, \tag{19}$$

where L_{ijlk} is the elasticity tensor, ℓ is a material length parameter and π_0 is a material strength parameter. The assumption underlying the uncoupled relation (19) is that the elastic properties are not affected by the density of geometrically necessary dislocations.

From Eqs. (13) and (15)

$$\sigma_{ij} = L_{ijkl} \varepsilon^{e}_{kl}, \qquad T_{ji} = \ell^2 \pi_0 \alpha_{ij} \tag{20}$$

and from Eq. (14)

$$\xi^{(\beta)}_i = \ell^2 \pi_0 e_{ipq} m^{(\beta)}_p \alpha_{rq} s^{(\beta)}_r. \tag{21}$$

We now confine attention to plane strain deformations with respect to the coordinates (x_1, x_2) under the assumption that $s^{(\beta)}_3 = 0$ and $m^{(\beta)}_3 = 0$ for all slip systems. Granted this, the two nonvanishing components of α_{ij} are

$$\alpha_{i3} = \sum_{\beta} s^{(\beta)}_i \partial^{(\beta)} \gamma^{(\beta)} \qquad (i = 1, 2), \tag{22}$$

where, for any slip system β, we write $\partial^{(\beta)}$ for the directional derivative with respect to the slip direction $s^{(\beta)}_i$, e.g.

$$\partial^{(\beta)} \Phi = \Phi_{,i} s^{(\beta)}_i, \qquad \partial^{(\beta)} \partial^{(\kappa)} \Phi = \Phi_{,ij} s^{(\beta)}_i s^{(\kappa)}_j. \tag{23}$$

From Eqs. (21), (22) and the orthogonality relation $s^{(\beta)}_i m^{(\beta)}_i = 0$

$$\xi^{(\beta)}_i = \ell^2 \pi_0 s^{(\beta)}_i \sum_{\kappa} S^{(\beta\kappa)} \partial^{(\kappa)} \gamma^{(\kappa)}, \tag{24}$$

where $S^{(\beta\kappa)}$ are the slip interaction coefficients

$$S^{(\beta\kappa)} = s^{(\beta)}_j s^{(\kappa)}_j. \tag{25}$$

During plastic flow (9) implies

$$\tau^{(\beta)} = \varphi^{(\beta)} \operatorname{sgn} \dot{\gamma}^{(\beta)} - \ell^2 \pi_0 \sum_{\kappa} S^{(\beta\kappa)} \partial^{(\beta)} \partial^{(\kappa)} \gamma^{(\kappa)} \tag{26}$$

and the stress rate–strain rate relation is

$$\dot{\sigma}_{ij} = L_{ijkl} \left[\dot{\varepsilon}_{kl} - \sum_{\beta} \frac{\dot{\gamma}^{(\beta)}}{2} (s^{(\beta)}_k m^{(\beta)}_l + s^{(\beta)}_l m^{(\beta)}_k) \right]. \tag{27}$$

Note the presence of two sources of hardening in the yield condition (26): dissipative hardening resulting from the temporal increase in the slip resistance $\varphi^{(\beta)}$ via Eq. (17) and energetic hardening represented by the final term in Eq. (26).

The slip resistance is taken to have the same initial value for all slip systems; this initial value is identified with the strength parameter π_0 in Eq. (20). Two descriptions of

the dissipative hardening are used: (i) to focus on the effect of the energetic term in Eq. (26), calculations are carried out using $h^{(\beta\kappa)} \equiv 0$ in Eq. (17), so that $\dot{\varphi}^{(\beta)} \equiv 0$ and $\varphi^{(\beta)} \equiv \pi_0$; (ii) in other calculations, the effect of dissipative hardening is accounted for by specifying

$$h^{(\beta\kappa)} = \begin{cases} H_0, & \kappa = \beta, \\ \rho H_0, & \kappa \neq \beta, \end{cases} \tag{28}$$

where H_0 and ρ are prescribed constants.

The elasticity is taken to be isotropic, characterized by Young's modulus E and Poisson's ratio ν, with the shear modulus given by $2\mu = E/(1+\nu)$. Thus, there are six material parameters that characterize the mechanical behavior: E, ν, π_0, H_0, ρ (in all calculations here $\rho = 1$) and ℓ. In addition, for each crystal the number of slip systems and the orientation of each as specified by $s_i^{(\beta)}$ ($s_i^{(\beta)} m_i^{(\beta)} = 0$) need to be given.

2.2. Numerical implementation

2.2.1. Spatial discretization

The finite element method is based on independent discretizations of the displacement field $u_i(x_1, x_2)$ and the slip field $\gamma^{(\beta)}(x_1, x_2)$. In each finite element, these fields are related to nodal values according to

$$\gamma^{(\beta)}(x_1, x_2) = \sum_{K=1}^{N} \phi^K(x_1, x_2) \Gamma_K^{(\beta)}, \tag{29}$$

$$u_i(x_1, x_2) = \sum_{K=1}^{N} \phi^K(x_1, x_2) U_i^K, \tag{30}$$

where N is the number of nodes per finite element, and U_i^K and $\Gamma_K^{(\beta)}$ are the nodal values of displacement and slip, respectively. Thus, the number of unknowns per node is two plus the number of slip systems. Eight node isoparametric quadratic elements with serendipity interpolation functions ϕ^K are used for both u_i and $\gamma^{(\beta)}$. As a consequence, u_i and $\gamma^{(\beta)}$ are continuous across element boundaries, but the derivatives $u_{i,j}$ and $\gamma_{,i}^{(\beta)}$ are not. Within each element the integrations in Eq. (6) are carried out using 3×3 point Gaussian integration.

For a representative finite element, we calculate

$$r_i^K = \int_{Be} \sigma_{ij} \phi_{,j}^K \, \mathrm{d}v - \int_{\partial Be_t} t_i \phi^K \, \mathrm{d}a, \tag{31}$$

$$R_K^{(\beta)} = \int_{Be} [(\tau^{(\beta)} - \pi^{(\beta)}) \phi^K - \xi_i^{(\beta)} \phi_{,i}^K] \, \mathrm{d}v + \int_{\partial Be_q} q^{(\beta)} \phi^K \, \mathrm{d}a \tag{32}$$

with the surface integrals appearing only if one or more sides of the element are on a surface where t_i or $q^{(\beta)}$ is prescribed.

Denoting the assembled force vectors from Eqs. (31) and (32) by $\mathbf{r}_i$ and $\mathbf{R}^{(\beta)}$, respectively, and noting that u_i and $\gamma^{(\beta)}$ can be varied independently, the principle of

virtual work (5) implies

$$\mathbf{r}_i \cdot \delta \mathbf{U}_i = \mathbf{0} \tag{33}$$

for $i = 1, 2$ and

$$\mathbf{R}^{(\beta)} \cdot \delta \boldsymbol{\Gamma}^{(\beta)} = \mathbf{0} \tag{34}$$

for β ranging over the number of active slips.

Relation (33) implies $\mathbf{r}_i = \mathbf{0}$, while in Eq. (34) $\delta \boldsymbol{\Gamma}^{(\beta)} = \mathbf{0}$ unless plastic loading occurs. Only when plastic loading occurs can $\delta \boldsymbol{\Gamma}^{(\beta)}$ be nonzero and in that case the corresponding $\mathbf{R}^{(\beta)}$ vanishes. An issue for the numerical implementation is that Eq. (34) is a discretization of a weak statement of the microforce balance (26) whereas the yield condition, (18), is a pointwise condition that, in the finite element context, is met at individual integration points within an element.

In the calculations here, the yield condition is evaluated at each Gauss point within an element. If the plastic loading condition is not met at a Gauss point, the contribution to Eq. (32) from that integration point is taken to be zero. This poses no special difficulty for evaluating Eq. (32) but, as discussed subsequently, the method for handling these integration points does affect the stability and convergence of the iterative procedure.

2.2.2. *Iteration procedure*

At a given stage of the loading history, we suppose that an equilibrium configuration is known. We denote the value of the time-like parameter characterizing the loading history at this known configuration by t. At this stage, the values of σ_{ij} and $\xi_i^{(\beta)}$ at integration points within each element and the nodal values U_i and $\Gamma^{(\beta)}$ satisfy Eqs. (33) and (34). An increment of loading is applied and the equilibrium configuration corresponding to the updated load, for which the value of the time-like parameter is $t + \Delta t$, needs to be calculated.

A predictor–corrector method is used with the first step based on assuming elastic response at each integration point. A good initial guess for the predicted nodal displacements speeds up convergence. To achieve this, the predicted displacements at the current stage of loading are obtained by linear extrapolation of the displacement history at each node (at nodes where displacement boundary conditions are imposed, the nodal values are required to be the imposed values). The displacement increment is then given by

$$\Delta U_i = U_i^{\text{extrapolated}} - U_i(t) \tag{35}$$

and the trial stress state, $\tilde{\sigma}_{ij}$, is obtained from

$$\Delta \sigma_{ij} = L_{ijkl} \Delta \varepsilon_{kl}, \quad \tilde{\sigma}_{ij} = \sigma_{ij}(t) + \Delta \sigma_{ij}, \tag{36}$$

where $\Delta \varepsilon_{kl}$ is calculated from Δu_k and, initially, the trial value of $\tilde{\xi}_i^{(\beta)}$ is identified with its previous known value.

The yield condition, (18), is then checked at each integration point using the trial stress state. If

$$|\tilde{\tau}^{(\beta)} + \tilde{\xi}_{i,i}^{(\beta)}| < \tilde{\varphi}^{(\beta)}, \tag{37}$$

where $\tilde{\tau}^{(\beta)}$ is calculated from $\tilde{\sigma}_{ij}$ using Eq. (7), then the material behavior at that integration point is elastic, otherwise it is plastic.

A tangent matrix, $\mathbf{A}$, is constructed from the derivatives

$$\frac{\partial \mathbf{r}_i}{\partial \mathbf{U}_i}, \quad \frac{\partial \mathbf{r}_i}{\partial \boldsymbol{\Gamma}^{\beta)}}, \quad \frac{\partial \mathbf{R}^{(\beta)}}{\partial \mathbf{U}_i}, \quad \frac{\partial \mathbf{R}^{(\beta)}}{\partial \boldsymbol{\Gamma}^{(\beta)}}$$

to obtain the set of linear equations for the increments $\Delta\mathbf{X} = [\Delta\mathbf{U}_i \,|\, \Delta\boldsymbol{\Gamma}^{(\beta)}]$

$$\mathbf{A} \cdot \Delta\mathbf{X} = -\mathbf{b} \tag{38}$$

with $\mathbf{b} = [\tilde{\mathbf{r}}_i \,|\, \tilde{\mathbf{R}}^{(\beta)}]$ where $\tilde{\mathbf{r}}_i$ and $\tilde{\mathbf{R}}^{(\beta)}$ are assembled from the element contributions in Eqs. (31) and (32) using the field quantities $\tilde{\sigma}_{ij}$ and $\tilde{\xi}_i^{(\beta)}$.

Expressions for the element tangent matrix are long and not revealing, and are not presented. A nonzero contribution to Eq. (32) and to the corresponding stiffness matrix terms occurs only when the response at an integration point is plastic. However, a zero value of a stiffness matrix element can result in spurious modes or divisions by zero during the solution procedure. These must be avoided for the iterative procedure to converge. To accomplish this, the contribution to the stiffness matrix from $\partial R_K^{(\beta)}/\partial \Gamma^{(\beta)}$ is evaluated at each integration point as if the material behavior at that point were plastic. Then, if the material behavior at the integration point under consideration is actually elastic, these stiffness matrix terms are multiplied by a factor ε, where $\varepsilon \ll 1$. It is important to emphasize that this procedure has no effect on the converged solution, since it does not alter the values of $\mathbf{r}_i$ or $\mathbf{R}^{(\beta)}$ in Eqs. (31) and (32).

The solution to Eq. (38) gives values of ΔU_i and $\Delta \Gamma_i$ at each node which are differences between successive iterations. From these, the values of $\Delta\varepsilon_{kl}$ and $\Delta\gamma^{(\beta)}$ are calculated at each integration point ($\Delta\gamma^{(\beta)} \equiv 0$ at integration points where the material behavior is elastic). The values of $\tilde{\sigma}_{ij}$, $\tilde{\xi}_i$ and, when dissipative hardening is included, $\pi^{(\beta)}$, are updated at each integration point of the finite element mesh using Eqs. (27) and (24) so that

$$\tilde{\sigma}_{ij} \leftarrow \tilde{\sigma}_{ij} + L_{ijkl}\left[\Delta\varepsilon_{kl} - \sum_{\beta} \Delta\gamma^{(\beta)} s_l^{(\beta)} m_k^{(\beta)}\right], \tag{39}$$

$$\tilde{\xi}_i^{(\beta)} \leftarrow \tilde{\xi}_i^{(\beta)} + \ell^2 \pi_0 s_i^{(\beta)} \sum_{\kappa} S^{(\beta\kappa)} \tilde{\partial}^{(\kappa)} \Delta\gamma^{(\kappa)} \tag{40}$$

and

$$\tilde{\pi}^{(\beta)} \leftarrow \tilde{\pi}^{(\beta)} + \sum_{\kappa} h^{(\beta\kappa)} \Delta\gamma^{(\kappa)}. \tag{41}$$

If the norm of $\mathbf{b}$, calculated using the updated values of $\tilde{\sigma}_{ij}$ and $\tilde{\xi}_i^{(\beta)}$, is less than a specified value, the field quantities of the trial solution are identified with those of the equilibrium state at $(t + \Delta t)$ and a new increment of loading is applied. Otherwise the iterative procedure is repeated from Eq. (37) with the updated trial values.

The algorithm used here is similar to numerical procedures used previously in nonlocal plasticity calculations, see De Borst and Mülhaus (1992) and Liebe and Steinmann

(2001), and differs from iterative algorithms in conventional plasticity in several ways: (i) unlike a classical return mapping algorithm, the plastic strain at an integration point does not only depend on variables at that point; (ii) convergence does not guarantee that the yield condition is satisfied at each integration point, but it is satisfied in the weak sense; and (iii) the displacement and the plastic slip are interpolated separately.

3. Results

Two boundary value problems are analyzed: simple shear of a constrained layer and a two dimensional model composite material subject to simple shear. Each of these has been analyzed using discrete dislocation plasticity (Cleveringa et al. (1997, 1998, 1999a) for the composite material problem and Shu and Fleck (1999) for the constrained layer problem). The dislocations are represented as line defects in a linear elastic continuum (see e.g. Nabarro, 1967; Hirth and Lothe, 1968) and the method of solution for boundary value problems is that in Van der Giessen and Needleman (1995) and Cleveringa et al. (1999b). All dislocations are edge dislocations and the dislocations move only by glide, with the magnitude of the glide velocity taken to be proportional to the Peach–Koehler force. New dislocations are generated by simulating Frank–Read sources and, in the model composite problem, interactions with obstacles representing forrest dislocations or small precipitates are considered.

The discrete dislocation calculations are carried out in an incremental manner. Each time step involves three main computational stages: (i) determining the forces on the dislocations, i.e. the Peach–Koehler force; (ii) determining the rate of change of the dislocation structure, which involves the motion of dislocations, the generation of new dislocations and their mutual annihilation; and (iii) determining the stress and strain state for the current dislocation arrangement.

In the constrained layer shearing problem, boundary layers develop and there is a much larger hardening in single slip than in double slip, Shu et al. (2001). For the model composite material, the aggregate stress–strain response depends sensitively on whether or not there is a vein of unreinforced matrix parallel to the shear direction. If such a vein exists, the aggregate stress–strain response is essentially that of the matrix and there is no size effect. On the other hand, when all slip planes are blocked, hardening is associated with the density of geometrically necessary dislocations needed to accommodate rotation of the reinforcement and, furthermore, there is a large Baushinger effect on unloading due to the internal stresses that develop, Cleveringa et al. (1997, 1998, 1999a). Here, the extent to which the nonlocal plasticity theory of Gurtin (2002) reproduces the features seen in these plane strain discrete dislocation calculations is explored.

3.1. Boundary layer in simple shear

Simple shear of a crystalline strip, of height h in the x_2-direction, is considered, with shearing along the x_1-direction as illustrated in Fig. 1. Plane strain and quasi-static loading conditions are assumed, and the strip is unbounded in the x_1- and x_3-directions.

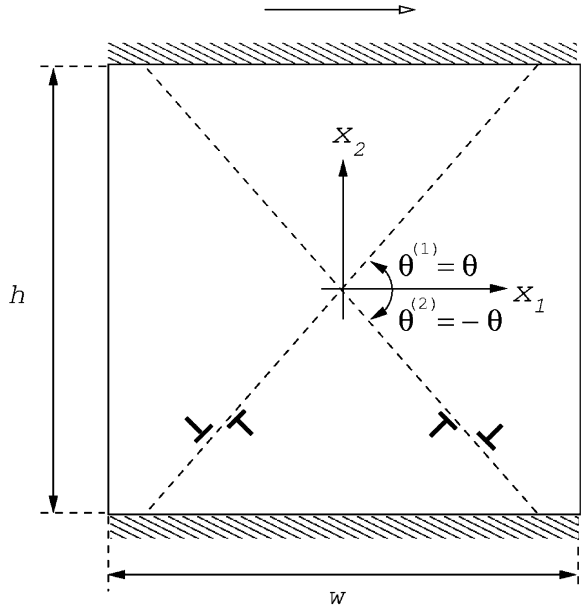

Fig. 1. Illustration of the problem formulation for simple shear of an elastic–plastic layer of thickness h with two active slip systems. Note that the coordinate system used in the analyses places the x_1-axis at the base of the strip.

The macroscopic boundary conditions are

$$u_1 = 0, \quad u_2 = 0 \quad \text{along } x_2 = 0,$$

$$u_1 = U(t) = h\Gamma(t), \quad u_2 = 0 \quad \text{along } x_2 = h, \tag{42}$$

where $\Gamma(t)$ is the prescribed shear. In the constrained layer problem we restrict attention to monotonic loading, so that the prescribed shear rate satisfies $\dot{\Gamma} > 0$.

In addition, all field quantities are required to be periodic in x_1 with period w; for example, $u_i(x_1, x_2) = u_i(x_1 + jw, x_2)$ for any integer j. For the local theory and for the discrete dislocation calculations, the only boundary conditions are (42) and periodicity. However, for the nonlocal theory microscopic boundary conditions are required. Here we specify micro-free boundary conditions on the sides and micro-clamped boundary conditions on the top and bottom of the region analyzed, i.e.

$$q^{(\beta)} = \xi_i^{(\beta)} n_i = 0 \quad \text{along } x_1 = \pm w, \tag{43}$$

$$\gamma^{(\beta)} = 0 \quad \text{along } x_2 = 0, h, \tag{44}$$

where $\beta = 1, 2, \ldots M$, with M being the number of slip systems.

3.1.1. An exact solution for symmetric double slip

Consider a crystal with two slip systems symmetrically oriented with respect to the coordinate axes, with the slip-plane orientation specified by the angle $\theta^{(\beta)}$, so that

(cf. Fig. 1)

$$\theta^{(1)} = -\theta^{(2)} \equiv \theta. \tag{45}$$

We consider solutions of this boundary-value problem that have field quantities independent of x_1. Macroscopic equilibrium requires that σ_{12} be spatially uniform. We seek solutions for which σ_{11} and σ_{22} vanish.

The solution of the elasticity problem is simple shear and the stress is spatially uniform. Thus the entire strip reaches yield at the same time. At subsequent times, which we discuss here, the entire body undergoes plastic flow.

The orientation of slip system (1) is given by

$$\mathbf{s}^{(1)} = \cos\theta\mathbf{e}_1 + \sin\theta\mathbf{e}_2, \quad \mathbf{m}^{(1)} = -\sin\theta\mathbf{e}_1 + \cos\theta\mathbf{e}_2 \tag{46}$$

and, for double-slip, system (2) has the analogous equation with θ replaced by $-\theta$. Recalling that the slip resistances are initially equal (to π_0), we have, by symmetry,

$$\gamma^{(1)} = \gamma^{(2)} \equiv \bar{\gamma}, \quad \tau^{(1)} = \tau^{(2)} \equiv \bar{\tau}, \quad \varphi^{(1)} = \varphi^{(2)} \equiv \bar{\varphi}. \tag{47}$$

We suppose that $|\bar{\gamma}|$ is monotonically increasing. We may then integrate (17) to arrive at

$$\bar{\varphi} = \pi_0 + 2H_0|\bar{\gamma}|. \tag{48}$$

The microforce balance (26) then reduces to

$$\frac{\mathrm{d}^2\bar{\gamma}}{\mathrm{d}x_2^2} - \lambda^2\bar{\gamma} = -F, \tag{49}$$

where

$$\lambda^2 = \frac{H_0}{\sin^4\theta\pi_0\ell^2}, \quad F = \frac{\bar{\tau} - \pi_0\,\mathrm{sgn}\,\bar{\gamma}}{2\sin^4\theta\pi_0\ell^2}, \tag{50}$$

where $\bar{\gamma} > 0$ for $\theta < \pi/4$ and $\bar{\gamma} < 0$ for $\theta > \pi/4$.

Assume first that there is no dissipative hardening ($H_0 = 0$, so that $\lambda = 0$). Then Eq. (49) and the boundary conditions (44) yield

$$\bar{\gamma} = \frac{F}{2}(x_2 h - x_2^2). \tag{51}$$

Hence, the slip distribution is quadratic regardless of the value of ℓ. The limit $\ell \to 0$ is singular; in this limit the gradient terms in the basic equations disappear and the microscopic boundary conditions (43) and (44) are meaningless.

Consider now the case with dissipative hardening ($H_0 > 0$). Then, by virtue of the boundary conditions, the differential equation (49) has the solution

$$\bar{\gamma} = \frac{F}{\lambda^2}\left[1 - \cosh\lambda x_2 - (1 - \cosh\lambda h)\frac{\sinh\lambda x_2}{\sinh\lambda h}\right] \tag{52}$$

and note that

$$\frac{F}{\lambda^2} = \frac{\bar{\tau} - \pi_0\,\mathrm{sgn}\,\bar{\gamma}}{2H_0}. \tag{53}$$

As before, the limit $\ell \to 0$ is singular; the solution for $\ell = 0$ has $\bar{\gamma}$ spatially constant. A scaling of the equations with respect to the length scale h shows that the behavior of solutions as $\ell \to 0$ is equivalent to their behavior as $h \to \infty$. Thus, to discuss the boundary layer that forms in this limit it is appropriate to consider the semi-infinite slab $0 \leqslant x_2 < \infty$ with the boundary conditions for $\gamma^{(\beta)}$ in Eq. (44) replaced by

$$\gamma^{(\beta)} = 0 \text{ along } x_2 = 0, \quad \partial\gamma^{(\beta)}/\partial x_2 \to 0 \text{ as } x_2 \to \infty. \tag{54}$$

In this case the solution of Eq. (49) is

$$\bar{\gamma} = \frac{F}{\lambda^2}(1 - \mathrm{e}^{-\lambda x_2}) \tag{55}$$

and a measure of the "thickness" of the boundary layer near $x_2 = 0$ is provided by

$$\lambda^{-1} = \sin^2\theta \sqrt{\frac{\pi_0}{H_0}}\,\ell. \tag{56}$$

Thus, both dissipative hardening (as represented by H_0) and energetic hardening (as represented by ℓ) are necessary for the formation of a boundary layer. The absence of dissipative hardening allows the two boundaries to interact, no matter how far apart they may be.

We now sketch the steps involved in determining the remaining fields. The only nonvanishing plastic strain is ε^p_{12}, which is computed using Eq. (2)

$$\varepsilon^{\mathrm{p}}_{12} = k\bar{\gamma}, \quad k = \cos^2\theta - \sin^2\theta = \cos 2\theta. \tag{57}$$

Similarly, by Eq. (7)

$$\bar{\tau} = k\sigma_{12}. \tag{58}$$

Next, using the elastic stress–strain relation (21), assumed isotropic, we find that

$$\sigma_{12} = 2\mu(\varepsilon_{12} - k\bar{\gamma}). \tag{59}$$

Averaging this equation with respect to x_2 over the interval $[0, h]$ (using a subscript "ave" to denote the average value) we find that, since σ_{12} is spatially constant and since, by Eq. (42), the average of ε_{12} over the interval $[0, h]$ is $\Gamma/2$,

$$\sigma_{12} = \mu(\Gamma - 2k\bar{\gamma}_{\mathrm{ave}}). \tag{60}$$

In the two cases studied, solutions (51) and (52) of the differential equation (49) each result in an explicit expression for $\bar{\gamma}$ as an affine function of $\bar{\tau}$, and in each case $\bar{\gamma}_{\mathrm{ave}}$ is easily computed. Thus eliminating σ_{12} from Eqs. (58) and (60) yields a single (linear) equation to be solved for $\bar{\tau}$. Knowing $\bar{\tau}$ the equations above can be used to compute σ_{12} and ε_{12}, which are the only remaining fields of interest.

Imposing the micro-free boundary condition $q^{(\beta)} = 0$ on $x_2 = 0, h$, leads to the condition that $\mathrm{d}\bar{\gamma}/\mathrm{d}x_2 = 0$ at $x_2 = 0, h$. The solution to Eq. (49) with $H_0 \neq 0$ is then the uniform slip state $\bar{\gamma} = F/\lambda^2$ (with $H_0 = 0$, $\bar{\gamma}$ is also constant). Hence, the choice of the micro-clamped boundary condition is key for the emergence of the boundary layer.

3.1.2. Numerical solutions

In the numerical calculations, crystals with one or two slip systems are considered, as sketched in Fig. 1, with the slip plane orientation specified by the angle $\theta^{(\beta)} = \pm\theta$. For the nonlocal plasticity theory, field quantities in the solution to this simple shearing boundary value problem are independent of x_1 and macro-equilibrium requires σ_{12} to be spatially uniform. As shown by the analytical solution, for symmetric double slip σ_{12} is the only nonvanishing in-plane stress component. On the other hand, in single slip, neither σ_{11} nor σ_{22} vanish.

In the discrete dislocation calculations in Shu et al. (2001) field quantities are not independent of x_1 and the results shown here for the discrete dislocation calculations are for the cell average shear-stress, σ_{12}^{ave}, and shear-strain, $\varepsilon_{12}^{\text{ave}}(x_2)$, i.e.

$$\sigma_{12}^{\text{ave}} = \frac{1}{w}\int_{-w/2}^{w/2} \sigma_{12}(x_1, h)\,\mathrm{d}x_1 \tag{61}$$

and

$$\varepsilon_{12}^{\text{ave}}(x_2) = \frac{1}{w}\int_{-w/2}^{w/2} \varepsilon_{12}(x_1, x_2)\,\mathrm{d}x_1. \tag{62}$$

Note that the average strain $\varepsilon_{12}^{\text{ave}}$ is a function of x_2 while σ_{12}^{ave} is the shear stress that is work conjugate to Γ.

In order to facilitate comparison with the discrete dislocation results in Shu et al. (2001), stress quantities in this Section are normalized by a reference value $\tau_{\text{ref}} = 50$ MPa. The value of the shear modulus is $\mu = 526\tau_{\text{ref}}$, Poisson's ratio is taken to be $\nu = 0.33$ and the flow strength is specified by $\pi_0 = 0.309\tau_{\text{ref}}$. Various values of the dissipative hardening parameter H_0 are used.

The overall shear stress versus shear strain response is shown in Fig. 2 for two calculations for a crystal with a single slip system oriented at $\theta^{(1)} = 60^\circ$ from the x_1-axis. In one calculation $h/\ell = 1.25$ and in the other $h/\ell = 125$. For comparison purposes, the elastic slope, the shear modulus μ, is also shown. The calculations shown in Fig. 2 are carried out with $H_0 = 0$. The plastic shear stress–shear strain response is nearly size independent with an effective shear stiffness of $\approx 0.75\mu$. This is in good agreement with the discrete dislocation calculations of Shu et al. (2001) as well as with their simple crack model for single slip.

The shear strain distributions shown in Fig. 3 for two values of deformation show the narrow boundary layers that develop in single slip. For the nonlocal theory, for both single slip and symmetric double slip, since the shear strain distribution for the nonlocal theory is independent of x_1 $\varepsilon_{12}^{\text{ave}}(x_2) = \varepsilon_{12}(x_2)$. Strain distributions are shown in Fig. 3 for both $h/\ell = 1.25$ and $h/\ell = 125$. There is very little size dependence and very good agreement with the distribution of $\varepsilon_{12}^{\text{ave}}$ from Shu et al. (2001). Single slip calculations were also carried out with $H_0/\tau_{\text{ref}} = 2$ and the results do not differ qualitatively from those shown in Figs. 2 and 3.

Overall shear stress–shear strain curves for a symmetrically double slipping crystal with $\theta = 60^\circ$ are shown in Fig. 4 for two values of the characteristic length ℓ and for two values of the dissipative hardening parameter H_0. Varying h/ℓ by a factor of 100 shows that a small increase of the overall hardening with decreasing size is predicted

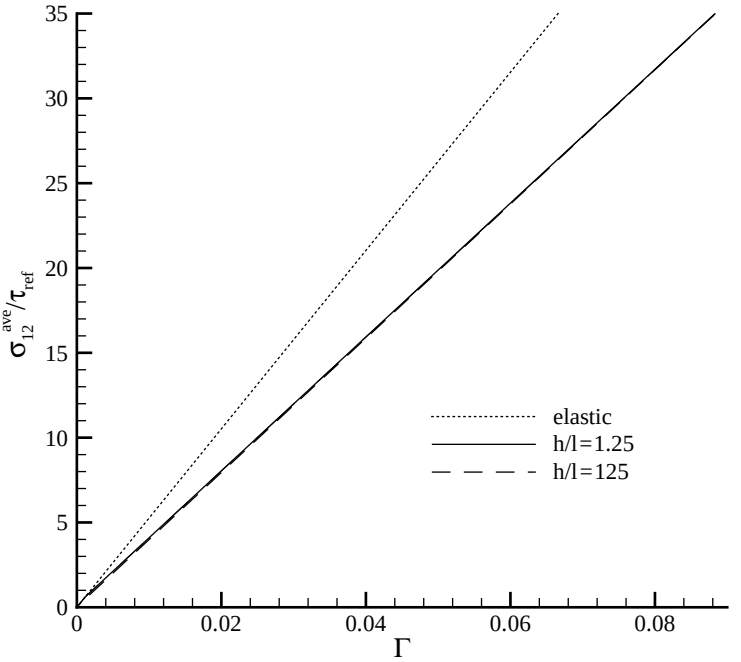

Fig. 2. Average shear stress response to the imposed shear strain Γ for single slip ($\theta^{(1)} = 60°$) with two values of the ratio of layer height h to material characteristic length ℓ. Micro-clamped boundary conditions, $\gamma^{(1)} = 0$, are imposed at $x_2 = 0, h$. For comparison purposes, a slope corresponding to the elastic shear modulus μ is also shown.

by the nonlocal theory. The discrete dislocation results in Shu et al. (2001) did not show a consistent trend for the variation in hardening with size scale. On the other hand, the discrete dislocation results did give rise to an increasing value of the back extrapolated flow strength [1] (Shu et al., 2001, Fig. 5) with decreasing size.

Fig. 5 shows the shear strain $2\varepsilon_{12} = \mathrm{d}u_1/\mathrm{d}x_2$ distribution for crystals with no dissipative hardening, i.e. $H_0 = 0$. The finite element and analytical solutions are coincident. There is nearly no size dependence exhibited by the shear strain distribution. In contrast, when there is a small amount of dissipative hardening, $H_0/\tau_{\mathrm{ref}} = 0.02$, Fig. 6 shows that the strain distribution is strongly size dependent. When the layer thickness is of the order of the material characteristic length, $h/\ell = 1.25$, the strain distribution is near the quadratic shape of the nonhardening crystal. On the other hand, for $h/\ell = 125$, the shear strain is essentially uniform across most of the layer, with boundary layers at the edges. At the scale in Fig. 6, the numerical and analytical solutions again coincide.

The effect of dissipative hardening at fixed size is shown in Fig. 7. Very slight dissipative hardening has a large effect on the predicted strain distribution, with the

[1] The back extrapolated flow strength is obtained by fitting a straight line to the hardening response and extrapolating back to a strain of 0.002.

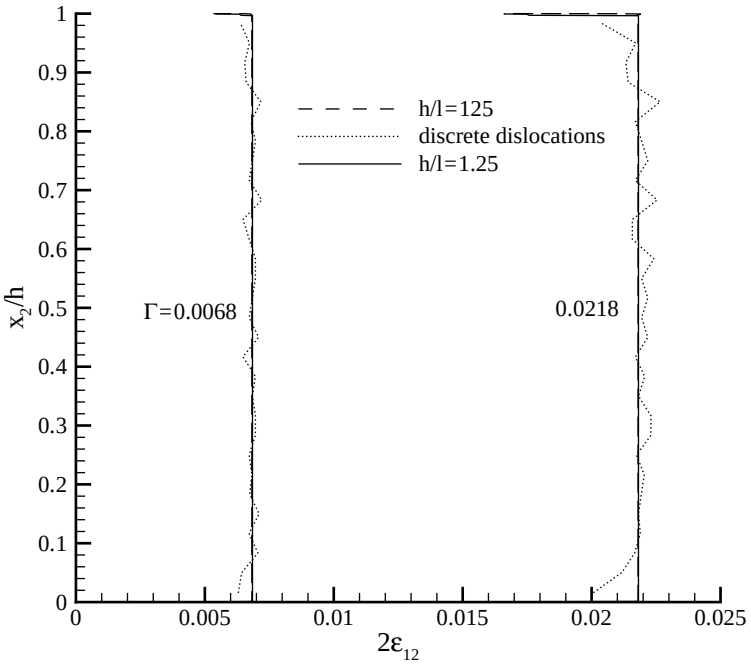

Fig. 3. Shear strain profiles at two values of overall shear strain Γ for single slip ($\theta^{(1)} = 60°$) with two values of the ratio of layer height h to material characteristic length ℓ; $\gamma^{(1)} = 0$ is imposed at $x_2 = 0, h$. Discrete dislocation strain profiles from Shu et al. (2001) are also shown.

strain being nearly uniform over most of the layer for $H_0/\tau_{\text{ref}} = 2$. Calculations of a constrained shear layer have been carried out (Fleck and Hutchinson, 2001; Niordson and Hutchinson, 2002) based on the isotropic nonlocal plasticity theory of Fleck and Hutchinson (2001) and a strong effect of dissipative hardening on the shear strain distribution is also found.[2]

Comparison with the discrete dislocation results of Shu et al. (2001) is shown in Figs. 8 and 9. The values $H_0/\tau_{\text{ref}} = 2$ and $h/\ell = 3.5$ give very good agreement with the average stress strain response and with the shear strain distributions. The evolution of the shear strain distribution is in remarkable agreement with that in the discrete dislocation calculations. In the calculations, $h = 1$ μm, so that $h/\ell = 3.5$ corresponds to $\ell = 0.286$ μm.

3.2. Model composite material

A planar model composite material consisting of elastic rectangular particles embedded in a plastically deforming matrix is subjected to simple shear as sketched in

[2] We are indebted to C.F. Niordson of the Technical University of Denmark for discussing unpublished results on the shear layer problem with us.

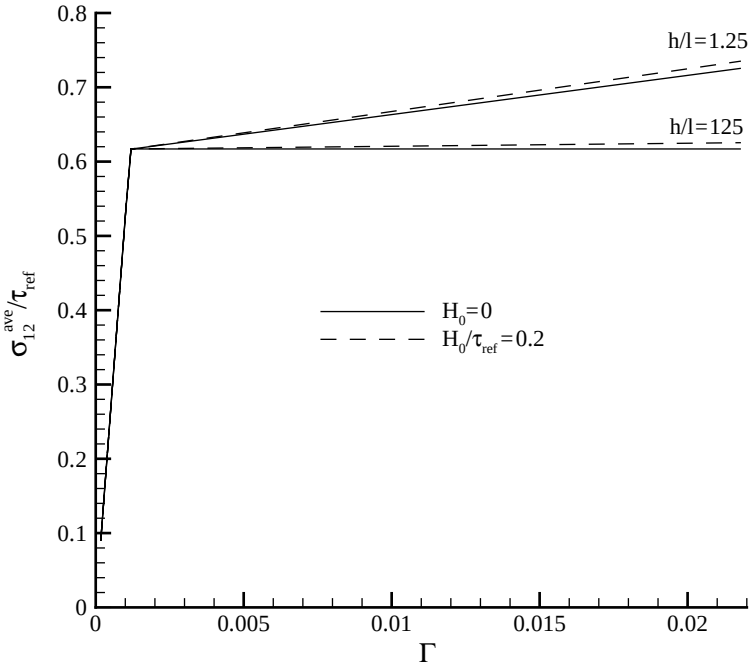

Fig. 4. Average shear stress response to the imposed shear strain Γ for double slip ($\theta^{(1)}=60°$, $\theta^{(2)}=-60°$) with two values of the ratio of layer height h to material characteristic length ℓ and two values of the slip system dissipative hardening H_0, with micro-clamped boundary conditions, $\gamma^{(1)}=\gamma^{(2)}=0$, are imposed at $x_2=0,h$.

Fig. 10. The geometrical parameters and the elastic properties of the matrix and of the reinforcement are the same as in Cleveringa et al. (1997, 1998, 1999a). The matrix material has a single slip system with the shearing direction parallel to the slip plane. Two reinforcement morphologies are considered, each having the same area fraction but different geometric arrangements of the reinforcing phase. In one morphology, termed material (i) in Cleveringa et al. (1997), the particles are square and are separated by unreinforced veins of matrix material while in the other, termed material (iii) in Cleveringa et al. (1997), the particles are rectangular and do not leave any unreinforced veins of matrix material.

The reinforcing particles are arranged in a hexagonal array, with each unit cell being of width $2w$ and height $2h$ ($w/h=\sqrt{3}$) (see Fig. 10). The particles are of size $2w_f\times 2h_f$; $h_f=w_f=0.416h$ for material (i) and $h_f=2w_f=0.588h$ for material (iii). In both cases, the reinforcement area fraction is 0.2.

The macroscopic boundary conditions on a unit cell are

$$u_1(t)=\pm h\Gamma(t), \quad u_2(t)=0 \text{ along } x_2=\pm h, \tag{63}$$

where for the composite problem unloading is considered so that $\Gamma(t)$ is not monotonically increasing.

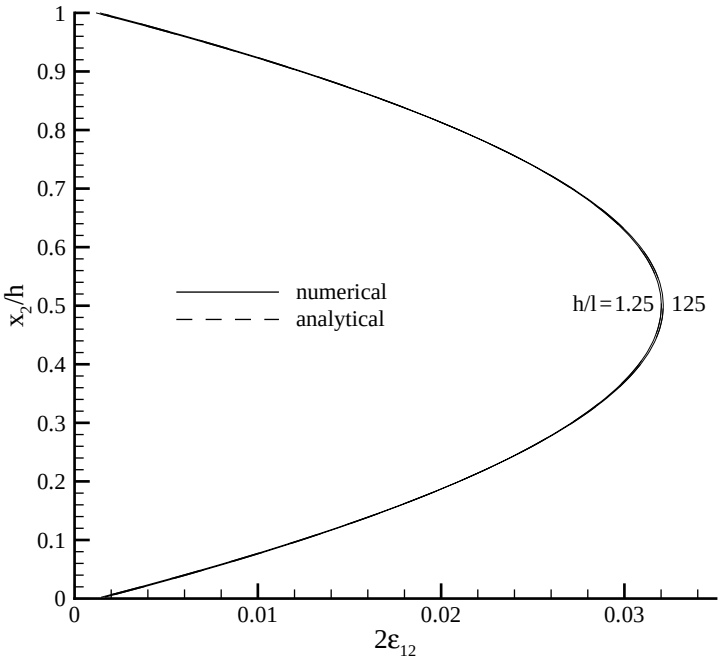

Fig. 5. Comparison of numerical and analytical shear strain distributions at $\Gamma = 0.0218$ for an ideally plastic ($H_0 = 0$) crystal with two slip systems ($\theta^{(1)} = 60°$, $\theta^{(2)} = -60°$). Micro-clamped boundary conditions, $\gamma^{(1)} = \gamma^{(2)} = 0$, are imposed at $x_2 = 0, h$.

Along the lateral sides ($x_1 = \pm w$) periodic macro-scale boundary conditions are imposed and the micro-scale boundary condition is taken to be $q^{(1)}(\pm w) = \xi_i^{(1)}(\pm w) n_i = 0$. Unless stated otherwise, the calculations are carried out using the micro-clamped boundary condition $\gamma^{(1)} = 0$ on the reinforcement–matrix interface. For comparison purposes, some calculations are carried out using the micro-free boundary condition $q^{(1)} = 0$ on the reinforcement–matrix interface.

Each phase is considered to be elastically isotropic, with shear modulus $\mu = 26.3$ GPa and Poisson's ratio $\nu = 0.33$ for the matrix; the corresponding values for the reinforcement are 192.3 GPa and 0.17, respectively. A value of $\pi_0 = 28$ MPa for the matrix and $h/\ell = 1.25$ was found to give good agreement with the monotonic stress–strain response obtained from the discrete dislocation calculations. A finite element mesh consisting of 384 bi-quadratic elements was used.

For the composite unit cell in Fig. 10

$$\sigma_{12}^{\text{ave}} = \frac{1}{2w} \int_{-w}^{w} \sigma_{12}(x_1, \pm h)\, \mathrm{d}x_1. \tag{64}$$

Overall shear stress versus shear strain curves for material (iii) are shown on Fig. 11 for ordinary, local crystal plasticity theory ($h/\ell = \infty$, $H_0 = 890$ MPa) and for the nonlocal theory with $h/\ell = 1.25$ and for both $H_0 = 0$ and $H_0 = 1$ MPa. For comparison

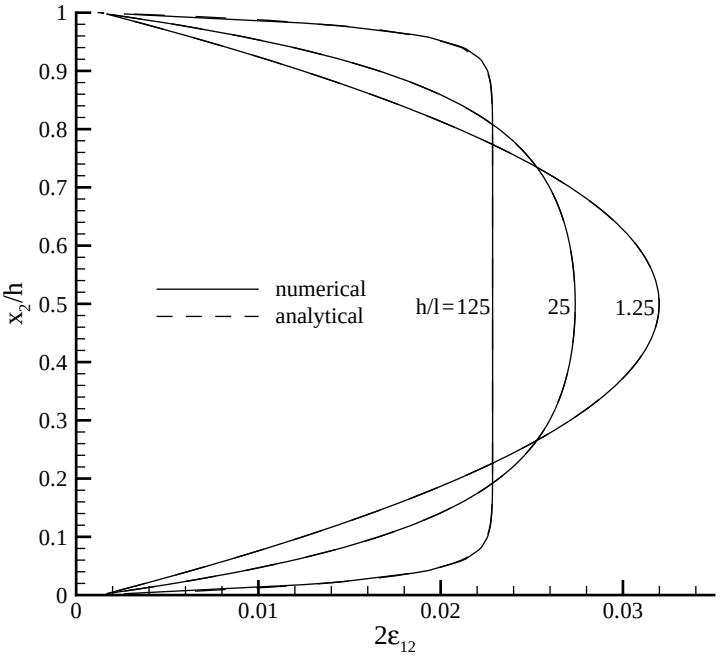

Fig. 6. Comparison of numerical and analytical shear strain distributions for double slip ($\theta^{(1)} = 60°$, $\theta^{(2)} = -60°$) with $H_0/\tau_{ref} = 0.02$ at $\Gamma = 0.0218$ for various values of the ratio of layer height h to material characteristic length ℓ. Micro-clamped boundary conditions, $\gamma^{(1)} = \gamma^{(2)} = 0$, are imposed at $x_2 = 0, h$.

purposes, the discrete dislocation results from Cleveringa et al. (1997, 1999a) are also plotted. A small amount of dissipative hardening, $H_0 = 1$ MPa, gives nearly the same stress–strain behavior as the calculation with H_0=0. Additional calculations using values of H_0 up to 200 MPa, not plotted, showed no significant change in the extent of the Bauschinger effect from what is seen in Fig. 11. In the calculations, $h = 1$ μm, so that $h/\ell = 1.25$ corresponds to $\ell = 0.8$ μm. This gives a very good fit to the loading curve, but somewhat underestimates the plastic deformation on load reversal. On unloading, both the discrete dislocation and the calculations based on Gurtin's (2002) nonlocal crystal plasticity theory exhibit a strong Bauschinger effect. The calculation based on local crystal plasticity theory, on the other hand, gives essentially an elastic response on unloading. In addition, unloading calculations carried out here using the nonlocal theory of Acharya and Bassani (2000) give the same, essentially elastic, unloading curve seen in Fig. 11 for the local theory.

The effect on the overall response of the micro-boundary conditions used at the matrix–reinforcement interface is shown in Fig. 12 for material (iii). Also shown for both sets of boundary conditions are results for $h/\ell = 12.5$. Although only the ratio h/ℓ matters, for the purposes of discussion, these will be considered as corresponding to an increase in physical size h with a fixed material length. The nonlocal plasticity theory predictions show that the hardening is reduced for the larger reinforcement, $h/\ell = 12.5$,

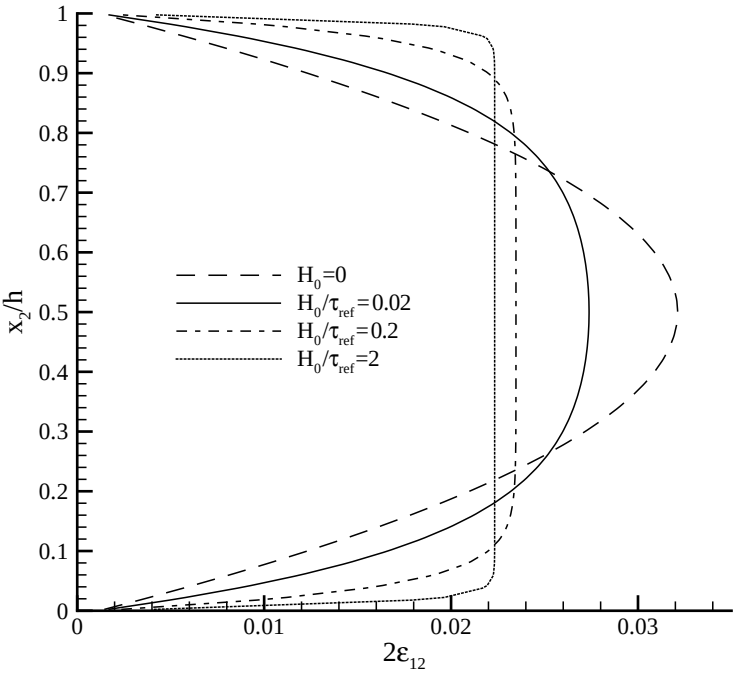

Fig. 7. Numerically computed shear strain distributions for double slip ($\theta^{(1)} = 60°$, $\theta^{(2)} = -60°$) with $h/\ell = 25$ at $\Gamma = 0.0218$ for various values of the slip system dissipative hardening H_0/τ_{ref}. Micro-clamped boundary conditions, $\gamma^{(1)} = \gamma^{(2)} = 0$, are imposed at $x_2 = 0, h$.

and that there is a considerable reduction in reverse plasticity. When the micro-boundary condition $q^{(1)}=0$ is imposed at the interface, as shown in Fig. 12b, the strain hardening with $h/\ell = 1.25$, is much less than in Fig. 12a and, when h/ℓ is increased to 12.5, the difference from the local solution is small. There is good agreement between the overall stress–strain curves obtained from the discrete dislocation calculations and the nonlocal calculations with the micro-clamped boundary condition $\gamma^{(1)}=0$ imposed at the particle–matrix interface. This comparison suggests that the appropriate boundary condition at the particle–matrix interface is the micro-clamped one.

Contours of slip, $\gamma^{(1)}$, for material (iii) are shown in Fig. 13. The stress levels at $\Gamma=0.0096$ are $\sigma_{12}^{\text{ave}}/\mu=2.74\times10^{-3}$ in Figs. 13a and 13b (corresponding to the stages of deformation from which unloading occurs in Fig. 11) and $\sigma_{12}^{\text{ave}}/\mu=2.20\times10^{-3}$ in Fig. 13c (the stage of deformation from which unloading occurs in Fig. 12b). For the local theory, $h/\ell = \infty$, in Fig. 13a slip is localized near the central reinforcement. On the other hand, for the nonlocal theory with $h/\ell = 1.25$, both with the micro-clamped, Fig. 13b, and the micro-free, Fig. 13c, boundary conditions slip is more spread out in the unit cell and slip bands away from the central reinforcement are seen, consistent with the displacement distributions seen in Cleveringa et al. (1997). The slip distribution reflects the rotation of the reinforcement (see Cleveringa et al., 1997), which requires the

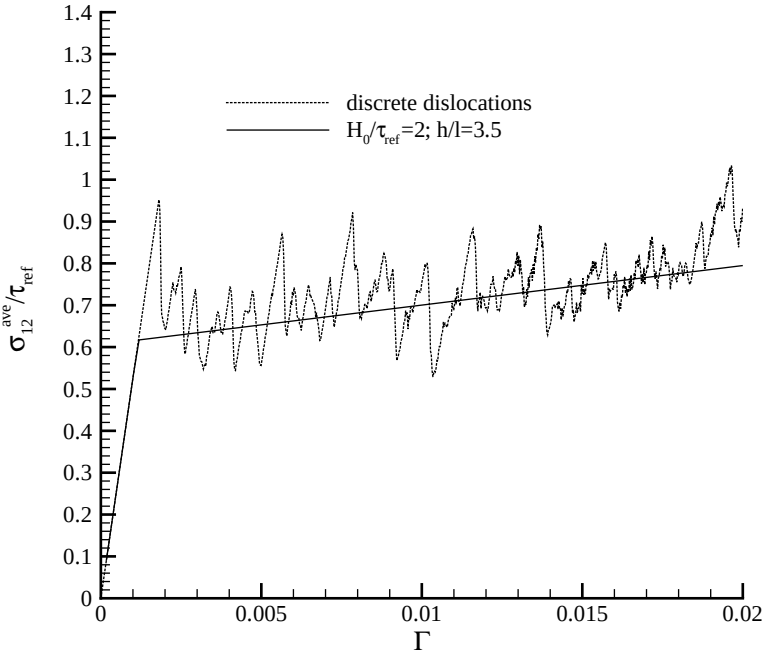

Fig. 8. Comparison of the discrete dislocation and nonlocal plasticity average shear stress response to the imposed shear strain Γ for double slip ($\theta^{(1)} = 60°$, $\theta^{(2)} = -60°$). The discrete dislocation data is from Shu et al. (2001).

presence of geometrically necessary dislocations near the reinforcement, Ashby (1970). In Fig. 14a, with the micro-clamped boundary condition, the contours of micro-stress $\xi_1^{(1)}$ reflect a density of geometrically necessary dislocations at the particle–matrix interface as seen in the discrete dislocation distribution for material (iii) in Cleveringa et al. (1997). For the micro-free boundary condition, Fig. 14b, the density of geometrically necessary dislocations is much lower and peaks away from the interface.

The aggregate stress–strain response for material (i) in Fig. 15 is essentially the same as for the matrix material. Furthermore, the response is neither sensitive to the choice of nonlocal boundary condition at the particle–matrix interface nor to the value of the material length scale. In addition, no Bauschinger effect is predicted. All these features are consistent with the discrete dislocation calculations although, as seen in Fig. 15 some Bauschinger effect does emerge from the discrete dislocation analysis but it is much smaller than for material (iii).

Fig. 16 shows slip contours for material (i). In these calculations $\pi_0 = 14$ MPa in order to fit the discrete dislocations results. The deformation is localized in a narrow band because of the vein of unreinforced matrix material (Fig. 16). Rotation of the central reinforcement is not required and the overall stress–strain response does not show any hardening. There are strong slip gradients in the x_2-direction, but this gradient is not associated with geometrically necessary dislocations and, hence, does not induce

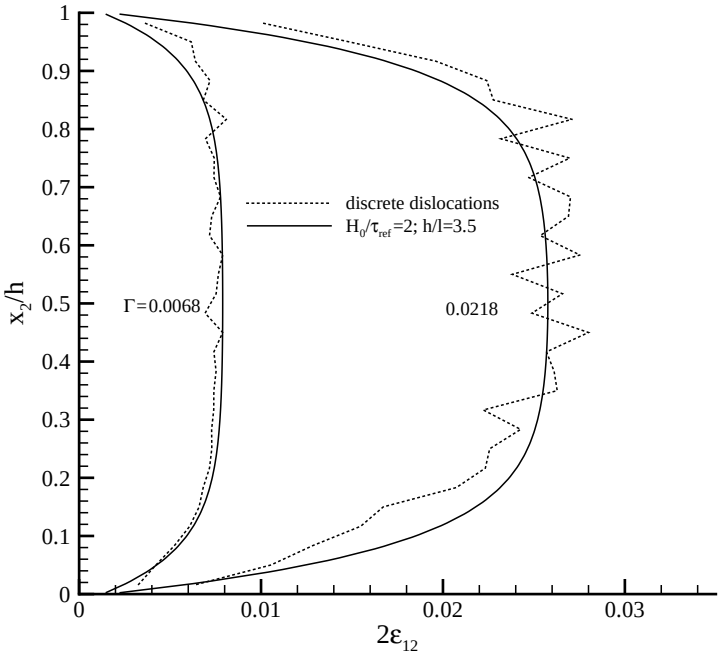

Fig. 9. Comparison of the discrete dislocation and nonlocal plasticity shear strain distributions at two values of imposed shear strain Γ for double slip ($\theta^{(1)} = 60°$, $\theta^{(2)} = -60°$) and with $\gamma^{(1)} = \gamma^{(2)} = 0$ imposed at $x_2 = 0, h$. The discrete dislocation data is from Shu et al. (2001).

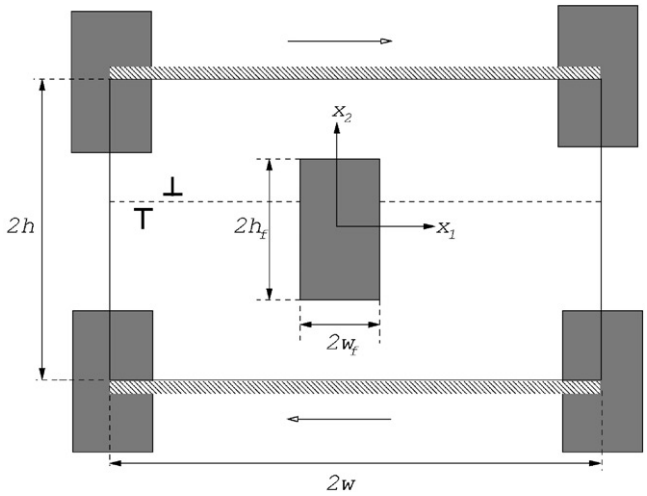

Fig. 10. Unit cell of a composite material with a doubly periodic array of elastic particles. All slip planes are parallel to the applied shear direction (x_1).

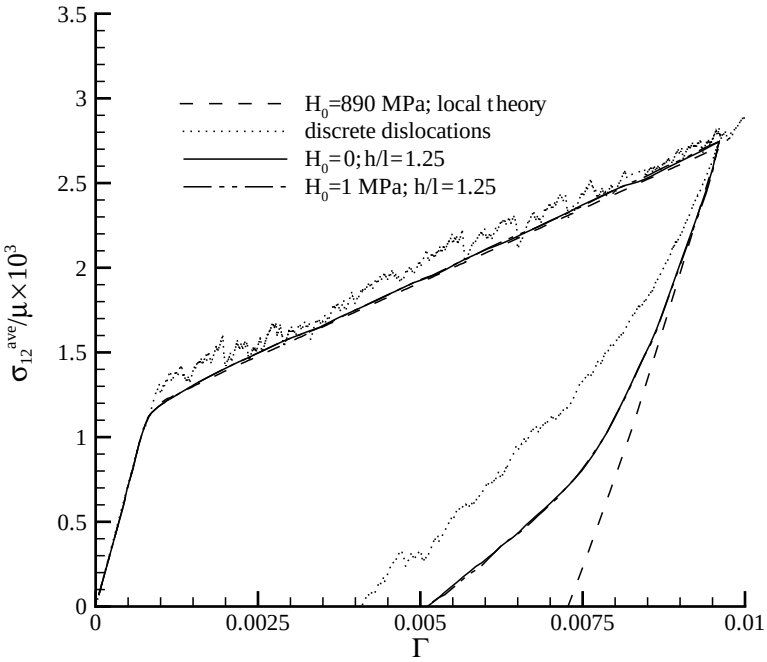

Fig. 11. Comparison of the discrete dislocation, local and nonlocal plasticity average shear stress, σ_{12}^{ave}, versus shear strain, Γ, curves for material (iii). Unloading from $\Gamma = 0.0096$ is also shown. The micro-clamped boundary condition, $\gamma^{(1)} = 0$, is imposed at the particle–matrix interface. The discrete dislocation data is from Cleveringa et al. (1999a).

energetic hardening. This illustrates the importance of only incorporating gradients associated with the density of geometrically necessary dislocations into the nonlocal constitutive description.

4. Discussion

The discrete dislocation simulations of Cleveringa et al. (1997, 1998, 1999a) and of Shu et al. (2001) highlight characteristic nonlocal effects that are a consequence of the presence of regions with a nonzero net Burgers vector, i.e. the presence of geometrically necessary dislocations. These effects include size-dependent stress–strain response, deformation boundary layers, morphology dependent hardening in multi-phase materials and internal stresses leading to (or enhancing) a Bauschinger effect on unloading. None of these features are exhibited by analyses based on a conventional, local theory of plasticity. The calculations here show that the nonlocal crystal plasticity theory of Gurtin (2002) captures these effects in remarkable detail.

The constrained shear layer problem has revealed a strong interaction between dissipative hardening and the predicted boundary layer. For an ideally plastic crystal with

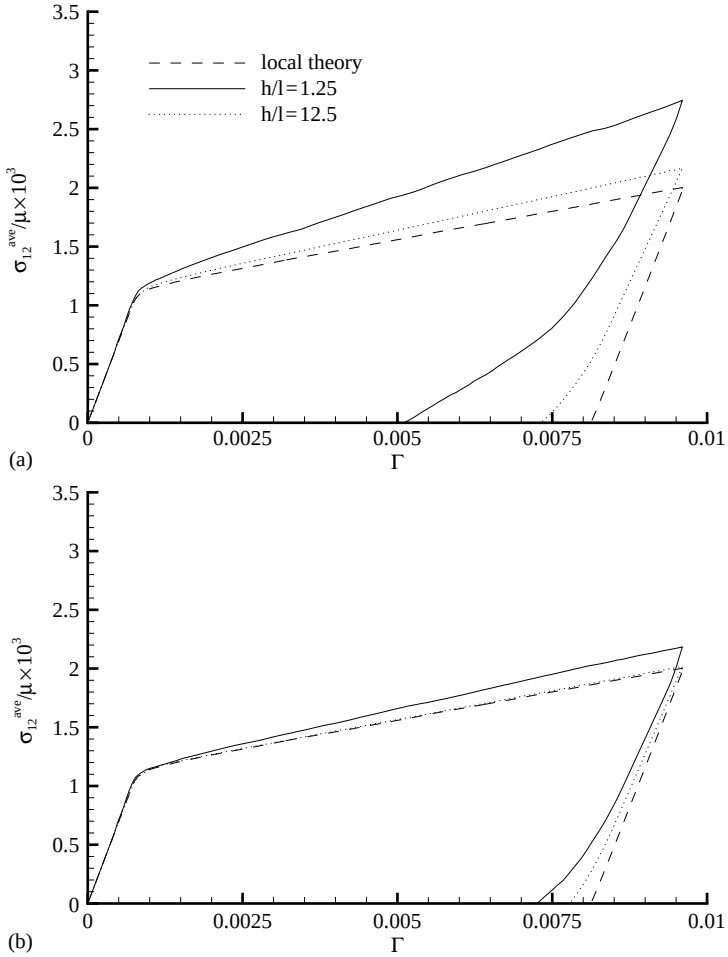

Fig. 12. Average shear stress, σ_{12}^{ave}, versus shear strain, Γ, curves for material (iii) with $H_0 = 0$ and various values of the ratio h/ℓ. (a) The micro-clamped boundary condition, $\gamma^{(1)} = 0$, is imposed at the particle–matrix interface. (b) The micro-free boundary condition, $q^{(1)} = 0$, is imposed at the particle–matrix interface.

two slip systems, a quadratic slip distribution occurs across the constrained layer regardless of the value of the material length scale. A small amount of dissipative hardening gives rise to a shear strain distribution that, for a sufficiently large value of the layer height, is nearly uniform except for boundary layers at the edges. The simple interpretation of this is that with hardening, the crystal attempts to deform in a uniform manner (as in a local description); but this uniformity is prevented near the boundaries because of the harder boundary layers forming there. The analytical solution shows the scaling of the boundary layer thickness with material properties (56) and reveals that the absence of dissipative hardening allows the two boundaries to interact regardless of

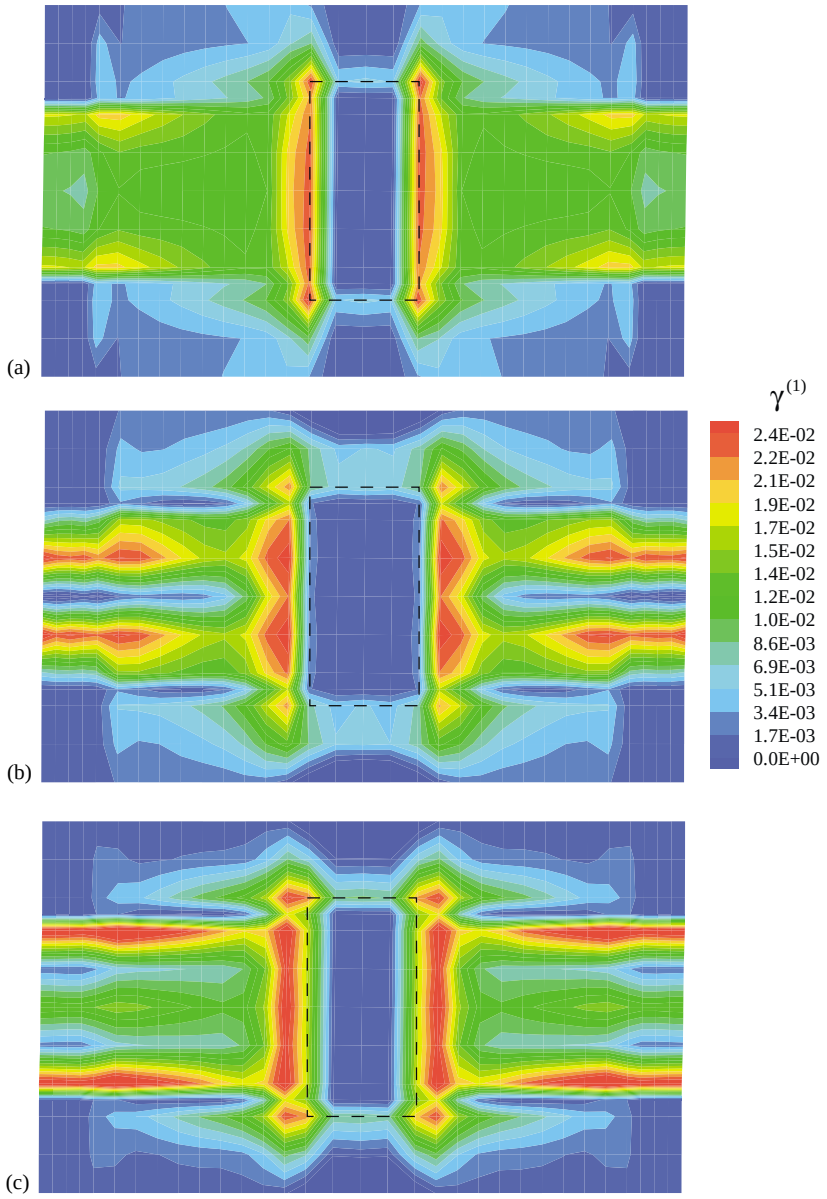

Fig. 13. Contours of slip $\gamma^{(1)}$ for morphology (iii) $\Gamma = 0.0096$. (a) Local plasticity theory, $h/\ell = \infty$, with $H_0 = 890$ MPa. (b) $h/\ell = 1.25$ and $H_0 = 0$ with the micro-clamped boundary condition $\gamma^{(1)} = 0$ at the particle–matrix interface. (c) $h/\ell = 1.25$ and $H_0 = 0$ with the micro-free boundary condition $q^{(1)} = 0$ at the particle–matrix interface.

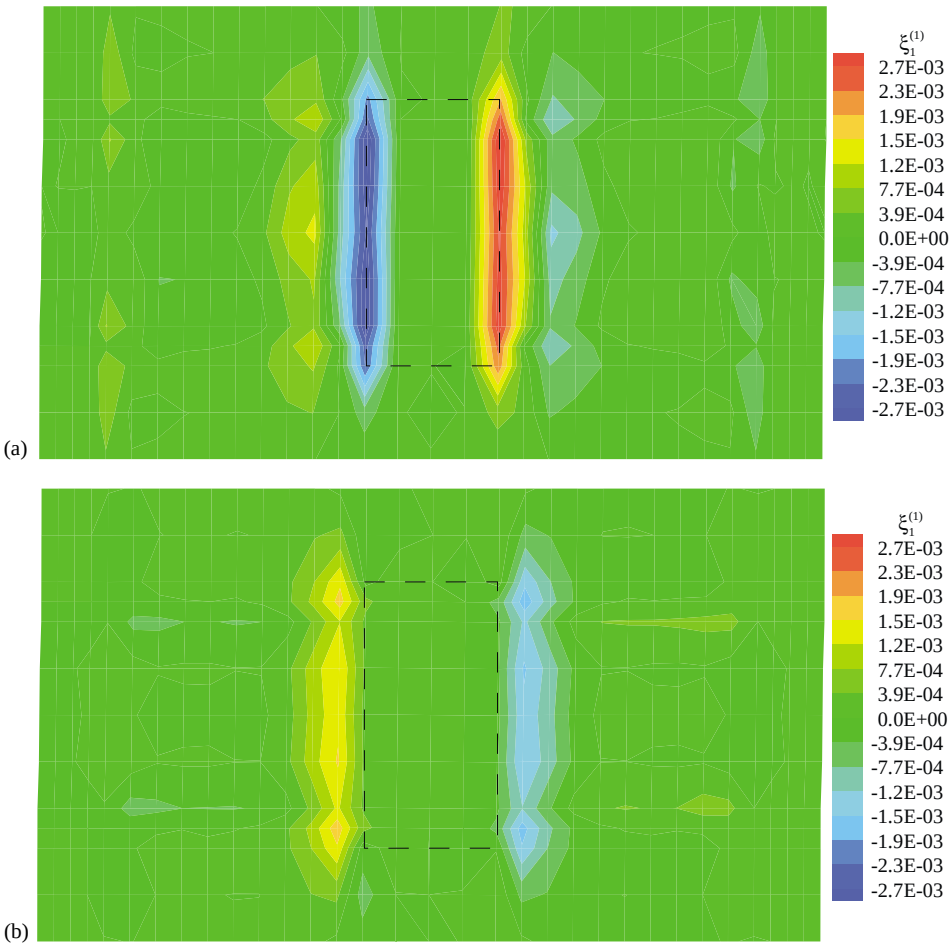

Fig. 14. Contours of microstress $\xi_1^{(1)}$ for morphology (iii) with $H_0 = 0$ at $\Gamma = 0.0096$. (a) $h/\ell = 1.25$ with the micro-clamped boundary condition $\gamma^{(1)} = 0$ at the particle–matrix interface. (b) $h/\ell = 1.25$ with the micro-free boundary condition $q^{(1)} = 0$ at the particle–matrix interface.

how far apart they are. In addition, the large difference in behavior seen in the discrete dislocation calculations in Shu et al. (2001) between crystals oriented for single slip and for double slip is reproduced by the nonlocal theory. Furthermore, an appropriate choice of material parameters gives excellent agreement with the discrete dislocation results for both the single slip and double slip orientations.

It is important to note that the dissipative hardening description in the calculations here is purely local. The nonlocal effects arise solely from a dependence of the free energy on the density of geometrically necessary dislocations. This gives an energetic contribution to hardening in the yield condition (26). Nonlocal effects can, of course, be included in the dissipative hardening description. However, for crystals undergoing

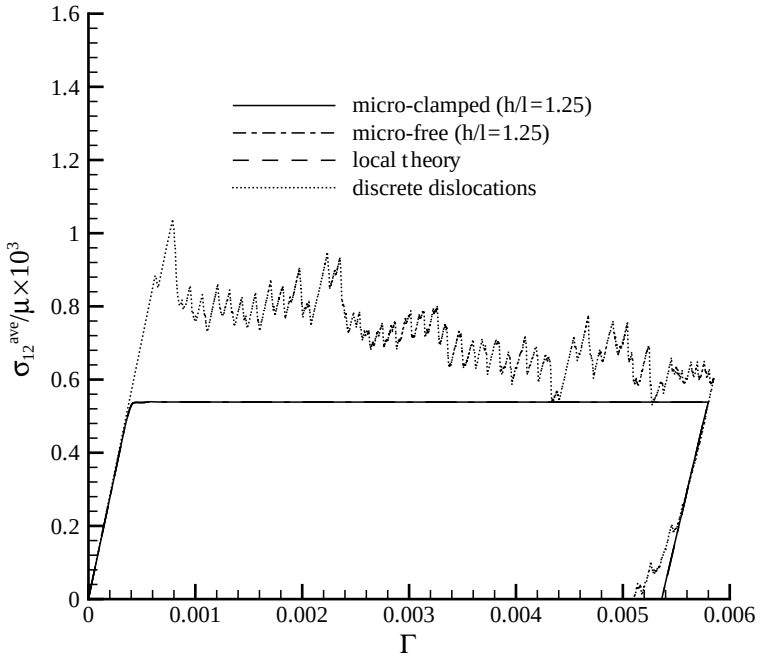

Fig. 15. Average shear stress, σ_{12}^{ave}, versus shear strain, Γ, curves for material (i) with both micro-clamped, $\gamma^{(1)} = 0$, and micro-free boundary conditions, $q^{(1)} = 0$, at the particle–matrix interface. Unloading from $\Gamma = 0.0058$ is also shown. The discrete dislocation behavior from Cleveringa et al. (1999a) and the local theory prediction are plotted for comparison purposes.

multislip, it is not at all clear as to how to aportion the effects of geometrically necessary dislocations among the various slip systems. To the extent that a local dissipative hardening description is adequate, this difficulty is avoided.

In the model composite material problem, the nonlocal theory of Gurtin (2002) exhibits a strong Bauschinger effect when the composite morphology is such as to require the development of a density of geometrically necessary dislocations. The simple theory of Acharya and Bassani (2000) can capture the effect of reinforcement morphology on the aggregate stress–strain response, as shown in Bassani et al. (2001), but not the Bauschinger effect on unloading. The reason for this is that the simple theory of Acharya and Bassani (2000) assumes that nonlocality affects only the dissipative hardening matrix.

The results also illustrate the strong effect of the choice of higher order boundary conditions. A particularly attractive feature of the theory presented in Gurtin (2002) is that the higher order boundary conditions are amenable to a physical interpretation. The condition $\gamma^{(\beta)} = 0$ signifies that the surface is hard in the sense that dislocations do not pass through it. On the other hand, the quantity $\xi_i^{(\beta)} n_i$ represents the microtraction work-conjugate to $\dot{\gamma}^{\beta}$ on the bounding surface and the condition that this traction vanish

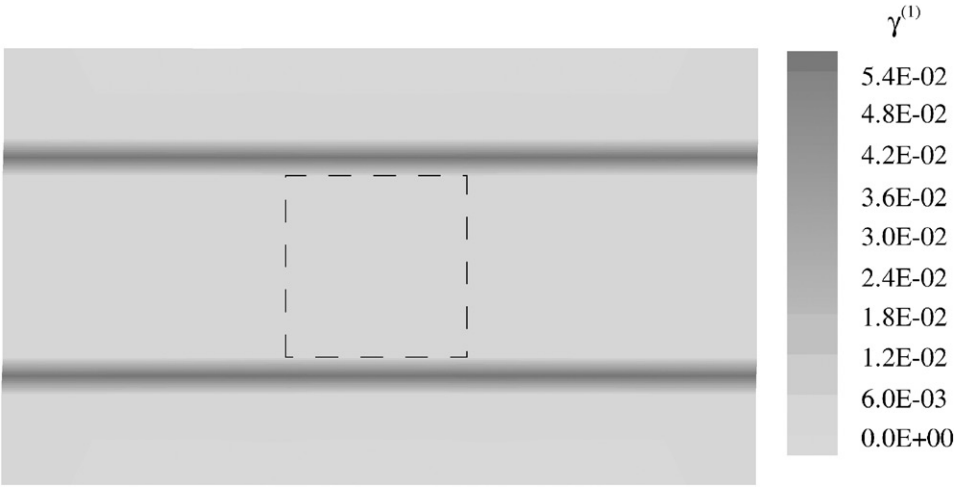

Fig. 16. Contours of slip $\gamma^{(1)}$ for morphology (i) at $\Gamma = 0.0058$ for $h/\ell = 1.25$ with the micro-clamped boundary condition, $\gamma^{(1)} = 0$, at the particle–matrix interface.

is tantamount to the condition that there is no force impeding slip on slip system (β) at the boundary.

Finally, it is worth noting that the problems considered here illustrate the importance of accounting for the discreteness of slip systems at small size scales. An isotropic theory can neither exhibit the dependence on the number of active slip systems seen in the shear layer problem nor the effect of reinforcement morphology in the composite problem (because this requires distinguishing the particular gradient of slip associated with geometrically necessary dislocations).

5. Conclusions

A finite element framework has been developed for solving boundary value problems using the nonlocal crystal plasticity theory of Gurtin (2002). The development has been restricted to infinitesmal deformations and rate independent material response. Two plane strain problems have been solved and the predictions of Gurtin's (2002) nonlocal theory have been compared with the results of discrete dislocation simulations.

- In the constrained shear layer problem, boundary layers and size effects can occur with uniform properties. Whether or not they emerge in the nonlocal theory depends on the higher order boundary conditions imposed.
- Both energetic and dissipative hardening play essential roles in the emergence of a boundary layer and in the size effect, as explicitly exhibited by the analytical solution of the nonlocal theory for symmetric double slip.

- The behavior seen in the discrete dislocation results for a constrained layer subject to simple shear is reproduced in detail by the nonlocal theory, including, for example, the boundary layer evolution and the difference in behavior between single slip and symmetric double slip orientations.
- The effect of reinforcement morphology on the stress–strain response of the model composite material is captured by the nonlocal theory for both loading and unloading.
- In the nonlocal plasticity calculations, the effect of geometrically necessary dislocations (net Burgers vector) enters only in the expression for the free energy; the description of the dissipative hardening is local. As a consequence, the problem of apportioning the measure of geometrically necessary dislocations among the various slip systems does not arise.

Acknowledgements

We are pleased to acknowledge support from the Materials Research Science and Engineering Center on *On Micro-and-Nano-Mechanics of Electronic and Structural Materials* at Brown University (NSF Grant DMR-0079964). In addition EB thanks the Brazilian Government for support through a CNPq Fellowship and MG acknowledges support from the National Science Foundation and the Department of Energy.

References

Acharya, A., Bassani, J.L., 2000. Incompatibility and crystal plasticity. J. Mech. Phys. Solids 48, 1565–1595.

Aifantis, E.C., 1984. On the microstructural origin of certain inelastic models. J. Eng. Mater. Technol. 106, 326–330.

Ashby, M.F., 1970. The deformation of plastically non-homogeneous materials. Philos. Mag. 21, 399–424.

Bassani, J.L., Needleman, A., Van der Giessen, E., 2001. Plastic flow in a composite: a comparison of nonlocal continuum and discrete dislocation predictions. Int. J. Solids Struct. 38, 833–853.

Brown, L.M., Ham, R.K., 1971. Dislocation–particle interactions. In: A. Kelly and R.B. Nicholson (eds) Strengthening Methods in Crystals. Elsevier, Amsterdam, pp. 12–135.

Busso, E.P., Meissonnier, F.T., O'Dowd, N.P., 2000. Gradient-dependent deformation of two-phase single crystals. J. Mech. Phys. Solids 48, 2333–2361.

Cleveringa, H.H.M., Van der Giessen, E., Needleman, A., 1997. Comparison of discrete dislocation and continuum plasticity predictions for a composite material. Acta Mater. 45, 3163–3179.

Cleveringa, H.H.M., Van der Giessen, E., Needleman, A., 1998. Discrete dislocation simulations and size dependent hardening in single slip. J. Phys. IV, 83–92.

Cleveringa, H.H.M., Van der Giessen, E., Needleman, A., 1999a. A discrete dislocation analysis of residual stresses in a composite material. Philos. Mag. A79, 863–920.

Cleveringa, H.H.M., Van der Giessen, E., Needleman, A., 1999b. A discrete dislocation analysis of bending. Int. J. Plasticity 15, 837–868.

De Borst, R., Mülhaus, H.-B., 1992. Gradient-dependent plasticity: formulation and algorithmic aspects. Int. J. Numer. Methods Eng. 35, 521–539.

De Guzman, M.S., Neubauer, G., Flinn, P., Nix, W.D., 1993. The role of indentation depth on the measured hardness of materials. Mater. Res. Symp. Proc. 308, 613–618.

Ebeling, R., Ashby, M.F., 1966. Dispersion hardening of copper single crystals. Philos. Mag. 13, 805–834.

Fleck, N.A., Hutchinson, J.W., 1993. A phenomenological theory for strain gradient effects in plasticity. J. Mech. Phys. Solids 41, 1825–1857.

Fleck, N.A., Hutchinson, J.W., 1997. Strain gradient plasticity. Adv. Appl. Mech. 33, 295–361.
Fleck, N.A., Hutchinson, J.W., 2001. A reformulation of strain gradient plasticity. J. Mech. Phys. Solids 49, 2245–2271.
Fleck, N.A., Muller, G.M., Ashby, F., Hutchinson, J.W., 1994. Strain gradient plasticity: theory and experiment. Acta Metall. Mater. 42, 475–487.
Gao, H., Huang, Y., Nix, W.D., Hutchinson, J.W., 1999. Mechanism-based strain gradient plasticity—I. Theory J. Mech. Phys. Solids 47, 1239–1263.
Gurtin, M.E., 2000. On plasticity of crystals: free energy, microforces, plastic strain gradients. J. Mech. Phys. Solids 48, 989–1036.
Gurtin, M.E., 2002. A gradient theory of single-crystal viscoplasticity that accounts for geometrically necessary dislocations. J. Mech. Phys. Solids 50, 5–32.
Hirth, J.P., Lothe, J., 1968. Theory of Dislocations. McGraw-Hill, New York.
Huang, Y., Gao, H., Nix, W.D., Hutchinson, J.W., 2000. Mechanism-based strain gradient plasticity—II. Analysis, J. Mech. Phys. Solids 48, 99–128.
Liebe, T., Steinmann, P., 2001. Theory and numerics of a thermodynamically consistent framework for geometrically linear gradient plasticity. Int. J. Numer. Methods Eng. 51, 1437–1467.
Ma, Q., Clarke, D.R., 1995. Size dependent hardness of silver single crystals. J. Mater. Res. 10, 853–863.
Mughrabi, H., 1983. Dislocation wall and cell structures and long-range internal stresses in deformed metal crystals. Acta Metall. 31, 1367–1379.
Nabarro, F.R.N., 1967. Theory of Crystal Dislocations. Oxford University Press, Oxford.
Niordson, C.F., Hutchinson, J.W., 2002. Non-uniform plastic deformation of micron scale objects. Technical Report, Harvard University.
Nye, J.F., 1953. Some geometrical relations in dislocated solids. Acta Metall. 1, 153–162.
Ortiz, M., Repetto, E.A., Stainier, L., 2000. A theory of subgrain dislocation structures. J. Mech. Phys. Solids 48, 2077–2114.
Shu, J.Y., Fleck, N.A., 1999. Strain gradient crystal plasticity: size-dependent deformation of bicrystals. J. Mech. Phys. Solids 47, 297–324.
Shu, J.Y., Fleck, N.A., Van der Giessen, E., Needleman, A., 2001. Boundary layers in constrained plastic flow: comparison of nonlocal and discrete dislocation plasticity. J. Mech. Phys. Solids 49, 1361–1395.
Stölken, J.S., Evans, A.G., 1998. A microbend test method for measuring the plasticity length scale. Acta Mater 46, 5109–5115.
Svendsen, B., 2002. Continuum thermodynamic models for crystal plasticity including the effects of geometrically-necessary dislocations. J. Mech. Phys. Solids 50, 1297–1329.
Van der Giessen, E., Needleman, A., 1995. Discrete dislocation plasticity: a simple planar model. Modell. Simul. Mat. Sci. Engin. 3, 689–735.